Sensors and Actuators B 228 (2016) 557–564

Contents lists available at ScienceDirect

Sensors and Actuators B: Chemical

journal homepage: www.elsevier.com/locate/snb

Analytical strategy to detect metal nanoparticles in mixtures without previous separation

Natalia L. Pacioni*, Alicia V. Veglia*

INFIQC–CONICET–Universidad Nacional de Córdoba, Departamento de Química Orgánica, Facultad de Ciencias Químicas, Haya de la Torre y Medina Allende s/n, X5000HUA, Ciudad Universitaria, Córdoba, Argentina

ARTICLE INFO

Article history:
Received 30 September 2015
Received in revised form
24 December 2015
Accepted 14 January 2016
Available online 19 January 2016

Keywords:
Gold nanoparticle
Silver nanoparticle
Rosolic Acid
Basic Fuchsin
Spectroscopic changes

ABSTRACT

Citrate-stabilized silver and gold nanoparticles were detected at the pmol L^{-1} level in aqueous mixtures without previous separation by using Basic Fuchsin (**BF**) as molecular probe. The method was validated by application to spiked drinking water. In addition, another acid-base indicator, Rosolic Acid (**RA**) permitted the semiquantitative detection of mixtures containing two different kinds of silver nanoparticles. The proposed strategy represents a fast, simple and cost-effective methodology to determine mixed metal nanomaterials, being sensitive to metal identity and ligands on the metal surface.

1. Introduction

For the last decade the use of nanomaterials in diverse areas such as imaging, catalysis, photocatalysis, data storage, biomedicine and optics has been growing rapidly [1–8]. On the other hand, research focused on environmental and health consequences associated to the increasing use of nanomaterials, such as metal nanoparticles (NP) is still in their infancy [9–12]. Their reliability as well as the establishment of new regulations for these emerging pollutants is closely related to the availability of analytical methods that permit, for example, to distinguish between different NP and quantify them. Nevertheless, there is not yet any standardized methodology to detect and evaluate engineered NP, for example in environmental samples [13].

Once NP are released into the environment their fate will be dictated mainly by physicochemical interactions occurring either with other nanoparticles or with natural water components present in an aquatic environment, assuming this scenery as their ultimate destiny [9,14].

Gold (AuNP) and silver (AgNP) nanospheres are currently the most employed metal NP due to their optical properties, relatively straightforward synthesis and good to great stability in colloidal solutions. As a consequence, finding these NP in natural environments will be highly probable in the future. Then, one great challenge that analytical chemists are currently facing is the development of analytical strategies to detect and quantify these kinds of NP in more complex mixtures [15–17].

Currently, analytical methods proposed to determine AgNP and AuNP are still scarce and they usually combine separation/preconcentration steps by different techniques such as Capillary Electrophoresis (CE) [14], (Asymmetric Flow) Field Flow Fractionation (FFF) [14,18,19], Cloud Point Extraction (CPE) [20–22] and Size Exclusion Chromatography [14,23] followed by detection using mainly Inductively Coupled Plasma-Mass Spectrometry (ICP-MS) [17] that usually involves digestion of the samples to get back the corresponding metal cations, or using Electrothermal Atomic Absorption Spectrometry (ETAAS) [22,24]. Although these methods can achieve detection limits at the ppt level, they require quite expensive instrumentation and high-skilled personnel to obtain good quality data (ICP-MS) [25], making these techniques not easily available for routine analysis in developing countries.

It is well known that organic compounds containing heteroatoms (S, N and O) interact strongly with the metal nanoparticle surface acting usually as ligands [26]. When these ligands are also dyes, the interaction with AuNP and AgNP results in a marked effect on the spectroscopic properties of the involved components

* Corresponding authors.
E-mail addresses: nataliap@fcq.unc.edu.ar, natiscba28@gmail.com (N.L. Pacioni), aveglia@fcq.unc.edu.ar (A.V. Veglia).

http://dx.doi.org/10.1016/j.snb.2016.01.064
0925-4005/

[27–30]. However, these spectroscopic modifications have not yet been exploited as strategies to detect the nanoparticles.

Here in, we describe an analytical strategy as an alternative method to detect AgNP and AuNP in aqueous mixtures. This approach consists in using two dyes usually employed as acid–base indicators, Basic Fuchsin (**BF**) or Rosolic Acid (**RA**) to interact with AuNP and AgNP. As a result of the interaction, absorption spectra are modified in a distinct manner if there is only one kind of NP present or a mixture of different NP.

As these changes are sensitive to the variation in NP concentration, using this strategy, citrate-stabilized nanoparticles (**AgNPc** and **AuNPc**) can be quantified in aqueous mixtures without previous separation. Also, it is possible to distinguish if a sample contains a mixture of citrate- and gallic acid-stabilized AgNP.

2. Experimental

2.1. Reagents and materials

4-[Bis(4-hydroxyphenyl)methylene]-2,5-cyclohexadienone (*p*-Rosolic Acid), gallic acid, hydrochloric acid 35–37%, sodium hydroxide and potassium monobasic phosphate were Merck. 4-(4-Aminophenyl(4-iminocyclohexa-2,5-dienylidene)methyl)-2-methylaniline (Basic Fuchsin) and trisodium citrate were Anedra. Methanol HPLC grade (Sintorgan), $HAuCl_4{\cdot}3H_2O$ (Aldrich), $AgNO_3$ (BioPack). All the reagents were used as received. MilliQ water was obtained from a Millipore instrument (resistivity, 25 °C: 18 MΩ cm).

2.1.1. Synthesis of gold and silver Nanoparticles

AuNP and AgNP were synthesized by two different synthetic methods described in literature [31,32] with slight modifications as indicated below, and characterized by UV–vis spectroscopy and electron microscopy (see Supplementary data, Fig. S1–S6).

2.1.1.1. Method 1, reduction using sodium citrate [31]. Usually, 50 mL of NP were prepared. For **AuNPc**, $HAuCl_4{\cdot}3H_2O$ (1.41 mmol L^{-1}) in MilliQ water was stirred and heated to reflux in an erlenmeyer. Then, $Na_3C_6H_5O_7$ (3.4 mmol L^{-1}) was added rapidly. The mixture was refluxed for 15 min. After cooling down to room temperature, the nanoparticles were stored overnight in a centrifuge tube. Aliquots of 5–6 mL were centrifuged at 4500 rpm for 30 min. The supernatant was discarded and the pellets were re-suspended in *ca.* 5 mL of MilliQ water.

For **AgNPc**, 1.00 mmol L^{-1} in $AgNO_3$ in Milli Q water was stirred and heated to reflux before $Na_3C_6H_5O_7$ (0.66 mmol L^{-1}) was added rapidly and refluxed for 20 min. The synthesized nanoparticles were stored in a plastic tube covered with aluminium foil. These AgNP were centrifuged at 3500 rpm for 30 min. Again, the supernatant was discarded and the pellets were re-suspended in *ca.* 5 mL of MilliQ water.

2.1.1.2. Method 2, reduction using gallic acid [32]. Briefly, for **AuNPg** 50 mL of an aqueous solution containing 0.27 mmol L^{-1} of $HAuCl_4$ and 88 μmol L^{-1} of gallic acid (added in the given order) were stirred for 30 min protected from light. Aliquots of 5–6 mL of the obtained pinkish solution were centrifuged at 3500 rpm for 30 min. The supernatant was discarded and the pellets were re-suspended in *ca.* 5 mL of MilliQ water. In a similar way, for **AgNPg** 50 mL of an aqueous solution containing 74 μmol L^{-1} of $AgNO_3$, 740 μmol L^{-1} of NaOH and 10 μmol L^{-1} of gallic acid were also stirred for 30 min protected from light. Then, aliquots of 5–6 mL of the obtained yellow solution were centrifuged at 8000 rpm for 30 min.

2.2. Instrumentation

All absorption spectra were measured in a UV–vis Shimadzu 1800 spectrophotomer in the 200–900 nm wavelength range using quartz cells (1 cm path-length). The pH was measured in an Orion (Boston, MA, USA) model 720 A pH-meter using a Ross combination pH electrode. The pH-meter was calibrated using standard buffers at pH 4.008 and 6.994.

Transmission Electron Microscopy images were obtained using a TEM-Jeol 1120 electron microscope, 80 kV accelerating voltage and Scanning Electron Microscopy measurements were performed in a SEM Zeiss, FE-SEM ∑igma, 15 kV accelerating voltage.

Zeta potentials were measured in a Delsa™Nano S Particle Analyzer (Beckman Coulter) at room temperature.

Raman spectra were obtained using a Horiba LabRaman confocal microscope with a 5 × (NA = 0.12) objective in the backscattering geometry. The exposition time was 10 s with a 4 cm^{-1} resolution and each spectrum corresponded to the average of 10. The excitation wavelength used was 514 nm corresponding to the laser line from Argon.

2.3. Characterization of nanoparticles

Particle size distributions were determined using TEM or SEM (see Supplementary data, Fig. S2–S6). These images were analyzed using ImageJ (W. S. Rasband, ImageJ, U. S. National Institutes of Health, Bethesda, Maryland, USA, http://rsb.info.nih.gov/ij/, 1997–2012). Briefly, 20 μL of the concentrated NP were delivered onto a carbon-coated copper grid (400 mesh, Electron Microscopy Sciences) for TEM or onto a carbon tape for SEM, and allowed to evaporate the solvent prior to imaging. NP with mean particle diameters of 12.8 nm (standard deviation: SD = 4.2), 25 nm (SD = 6.6) and 27.8 nm (SD = 6.0) for **$AuNPc_{13}$**, **$AuNPc_{25}$**, **$AuNPc_{28}$**, respectively; 52 nm and 55 nm (SD = 19) for **$AgNPc_{52}$**; 29 nm (SD = 12) and 4.6 nm (SD = 2.6) for **$AgNPg_{29}$** and **$AgNPg_{5}$**, respectively; and 55 nm (SD = 13) for **$AuNPg_{55}$** were used in this work. For AuNP, sizes determined by TEM were in accordance within error to those determined using Haiss' method [33]. In all cases the subscript indicates the NP size.

Absorption spectra (Fig. S1) revealed the surface Plasmon resonance band (SPR) positions were at 410, 418, 430, 520, 527 and 542 nm for **$AgNPg_5$**, **$AgNPg_{29}$**, **$AgNPc_{52}$**, **$AuNPc_{13}$**, **$AuNPc_{25}$** and **$AuNPg_{55}$**, correspondingly. Zeta potential values were in the range −20 to −30 mV, indicating colloidal stability of the suspensions.

2.4. General procedure

Stock solutions of **RA**, *ca.* 10 mg in 10 mL were freshly prepared in methanol. **BF** *ca.* 10 mg in 100 mL was dissolved in water and kept at 4 °C in a fridge. Both dyes solutions were covered with aluminium foil to avoid photodegradation [34]. Concentration was checked by UV–vis before using in experiments with NP.

2.4.1. Interaction of *RA* and *BF* with nanoparticles

First, 5.00 mL solutions containing a given concentration of NP were prepared by adding a selected volume (usually 150 μL) of a stock NP solution to different amounts of the dyes with concentrations in the range 0–120 μmol L^{-1} for **RA** or 0–16 μmol L^{-1} for **BF**.

In the case of **RA**, the solutions always contained 3% V/V of methanol in the corresponding buffer (10 mmol L^{-1} citrate buffer pH 5.03 or 10 mmol L^{-1} phosphate buffer pH 7.97). Spectra of the dyes in the presence of NP were compared to those without NP.

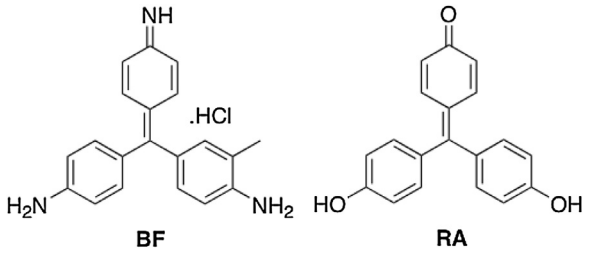

Scheme 1. Chemical structures for **BF** and **RA**.

2.4.2. Detection of mixtures of NP

RA (50 μmol L^{-1} at pH 7.97 and 100 μmol L^{-1} at pH 5.03) solutions containing a fixed amount of one kind of NP (**AgNPc$_{52}$**; **AgNPg$_5$** or **AuNPc$_{13}$**) and a variable concentration of another type of NP were prepared in 5.00 mL volumetric flasks with and without **RA**, as well as a solution of **RA** alone. Then, the absorption spectra were recorded.

2.4.3. Calibration curves

Standard solutions were prepared by duplicate as follows: four sets of mixtures of **AgNPc$_{52}$** and **AuNPc$_{13}$** were prepared by keeping constant the concentration of **AgNPc$_{52}$** (at two levels of concentration: 0.03 and 0.10 nmol L^{-1}) or the concentration of **AuNPc$_{13}$** (at two levels of concentration: 0.20 and 0.44 nmol L^{-1}) while varying the another NP concentration in the 0.064–1.30 nmol L^{-1} range for **AuNPc$_{13}$** and 0.008–0.107 nmol L^{-1} range for **AgNPc$_{52}$**, respectively. Concentrations of nanoparticles were estimated according to literature procedures [30,35]. All the solutions were 5 μmol L^{-1} in **BF**.

2.4.4. Recovery in drinking water

Drinking water was used without any pre-treatment. Blank solution did not show any signal for **AgNPc** or **AuNPc**. Then, solutions of **AgNPc$_{52}$** (0.003–0.022 nmol L^{-1}) containing **AuNPc$_{28}$** (0.024 nmol L^{-1}); 5% (v/v) drinking water and **BF** (5 μmol L^{-1}) were prepared by triplicate and their absorption spectra recorded and analyzed.

2.5. Surface Enhancement Raman Spectroscopy

All measurements were performed at room temperature and were calibrated to H_2O bands in the colloidal solutions. SERS spectra were recorded for 5 μmol L^{-1} **BF** in the absence and presence of **AuNPc$_{13}$** (0.2 nmol L^{-1}) or the presence of **AgNPc$_{52}$** (0.03 nmol L^{-1}).

3. Results and discussion

*3.1. Interaction of **RA** and **BF** with different metal nanoparticles: effect on absorption spectra*

As mentioned in Section 1, organic compounds containing in their chemical structure heteroatoms such as O, N and S interact with the metal nanoparticle surface, and this interaction can be evidenced by spectroscopic changes [27,30,36,37]. Generally, these modifications are more significant when a strong resonance coupling between the organic adsorbate and the NP occurs, a phenomenon dependent on the overlapping between the SPR and the molecular absorption peak [27]. Thus, we chose to use **RA** and **BF** because they have in their structure heteroatoms in the forms of −OH and $-NH_2$, respectively (Scheme 1). Besides, they are dyes absorbing close or in the SPR region of AgNP and AuNP (see Fig. S7 in Supplementary data) and in addition they are well-known acid–base indicators easily found in any lab.

The UV–vis spectra over the pH range from 3 to 12 did not show any spectroscopic differences for **BF** (pK_a < 3), while for **RA** we determined spectrophotometrically (not shown) a pK_a value of 7.0 ± 0.2. So, we chose to carry out all experiments with **BF** in its basic form (deionized water pH ≈6), as metal nanoparticles are usually not stable in strong acidic media (pH <3).

In the case of **RA** we worked at pH values where the predominant species was the acid (pH 5.03, phenolic form) or the base (pH 7.97, phenolate form). Moreover, no spectroscopic differences were observed with the chemical buffer identity (10 mmol L^{-1} citrate or 10 mmol L^{-1} phosphate) at a fixed pH. In 3% v/v methanol: citrate buffer pH 5.03, the acid **RA** species presents a maximum absorption (λ_{max}) at 474 nm [ε/mol^{-1} L cm^{-1}: (22.2 ± 0.6) × 10^2] while in 3% v/v methanol: phosphate buffer pH 7.97 the λ_{max} for the basic **RA** species is located at 535 nm [ε/mol^{-1} L cm^{-1}: (19.8 ± 0.5) × 10^2]. In the case of **BF**, the λ_{max} in water is 543 nm [ε/mol^{-1} L cm^{-1}: (63 ± 1) × 10^3 mol^{-1} L cm^{-1}].

Although it is difficult to predict what ligand and shape the NP will have in real samples, we selected to work with citrate-stabilized gold and silver nanospheres as models as they are the most widely used in applications involving aqueous systems. We also decided to compare them with NP containing a different ligand such as gallic acid, a well-known antioxidant used as additive in food and pharmaceutical industries [38]. Also, we would like to point out that average NP sizes employed in this work are commonly obtained using the mentioned synthetic methods (see Section 2.1.1) [31,32].

First, we evaluated the effect of the interaction between the NP and the molecular dyes on the absorption spectra of both components. Thus, the difference spectra (ΔAbs) obtained as the mixture's absorption spectrum (Abs dye@NP) minus the dye spectrum (Abs dye) were contrasted with the NP absorption spectrum (Abs NP). In addition, we analyzed the "net effect" (ΔAbs_{net}) obtained by subtracting the Abs NP from the ΔAbs. In the absence of any interaction between the dye and the NP, the ΔAbs_{net} should be null. We tried different dye concentrations as mentioned in Section 2 and selected to continue working with the minimum dye concentration that give us an observable ΔAbs_{net} (>10%) and its absorption in the absence of NP was ≥0.2 in order to minimize the spectrophotometric error.

*3.1.1. Interaction with neutral **RA***

At pH 5.03 (Fig. 1A), ΔAbs for **RA@AuNPc$_{13}$** showed a red-shifted and broader band respect to the **AuNPc$_{13}$** SPR that was better evidenced looking at the net effect (Fig. 1A inset). This spectroscopy change was attributed to NP agglomeration provoked by predominant van der Waals forces between NP [39] covered by the neutral **RA** respect to repulsive interactions [39] between NP covered by the negative charged citrate ligand. TEM images were in agreement with this phenomenon (Fig. 2A). In spite of agglomeration, no flocculation of NP was observed within the time of the experiments. The same effect was also observed for **AuNPc$_{25}$** (not shown) with a larger SPR broadening.

In contrast, **AgNPc$_{52}$** showed depletion of the extinction at the SPR (Fig. 1A) that might be product of either modification of the extinction coefficient due the interaction with **RA** or partial oxidation of the nanomaterial, though rationalization of this phenomenon is out of the scope of the present work. A similar behavior was also observed for **AgNPg$_5$** and **AgNPg$_{29}$** (not shown) while for **AuNPg$_{55}$** a decrease in the **RA** absorption wavelength region was noticed with no indication for NP agglomeration at larger wavelengths (see Supplementary data, Fig. S8). As **AuNPg$_{55}$** were more polymorphous, the observed effect cannot be attributed only to size and ligand identity.

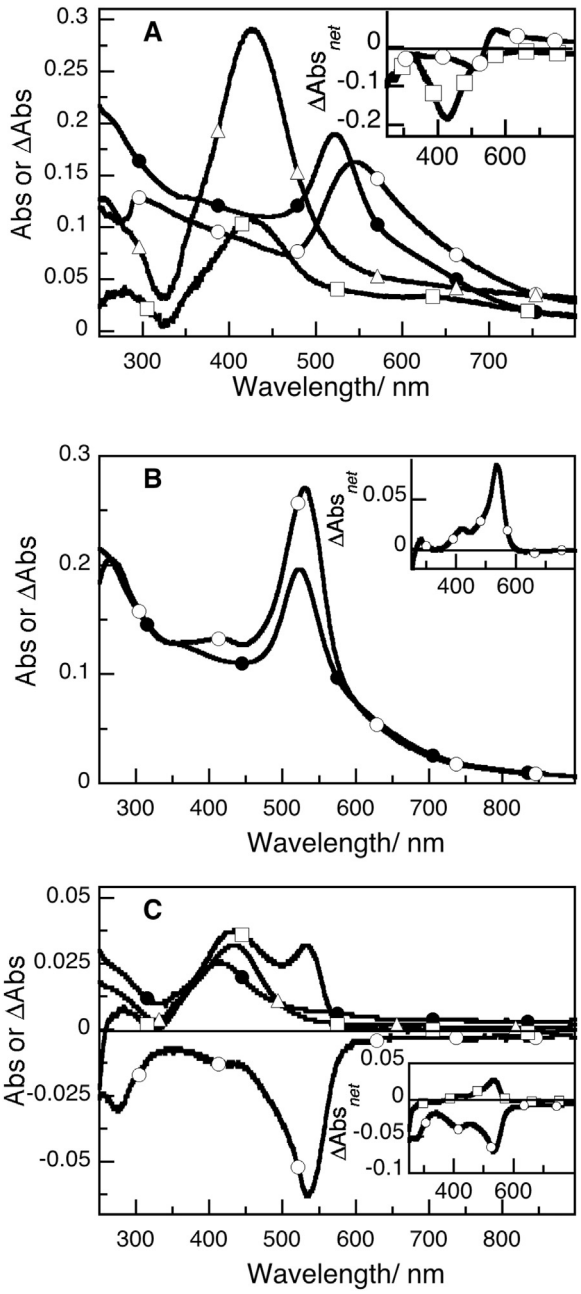

Fig. 1. (A) Absorption spectra for (●) **AuNPc$_{13}$** (0.81 nmol L^{-1}), (△) **AgNPc$_{52}$** (0.078 nmol L^{-1}) and their corresponding ΔAbs spectra for (○) **AuNPc$_{13}$** and (□) **AgNPc$_{52}$** obtained with 100 μmol L^{-1} **RA** at pH 5.03. (B) Absorption spectra for (●) **AuNPc$_{13}$** (0.81 nmol L^{-1}) and its corresponding ΔAbs spectra (○) obtained with 50 μmol L^{-1} **RA** at pH 7.97. (C) Absorption spectra for (●) **AgNPg$_5$**(0.47 nmol L^{-1}), (△) **AgNPc$_{52}$** (0.009 nmol L^{-1}) with their corresponding ΔAbs spectra (○) **AgNPg$_5$** and (□) **AgNPc$_{13}$**, respectively. In all cases insets show the corresponding ΔAbs_{net}.

3.1.2. Interaction with *RA* anion

At pH 7.97 **RA** is negative charged, prone to interact stronger with the NP surface. In the case of **AuNPc$_{13}$**, ΔAbs_{net} showed an increase in the extinction of **RA** (Fig. 1B) and no agglomeration of NP was observed in TEM images (Fig. 2B). This clearly indicates the basic species of **RA** stabilizes the **AuNPc** from aggregation in contrast to the effect observed at pH 5.03. In addition, enhancement of the extinction of **RA** can be attributed to plasmonic effects in the vicinity of the metal surface as observed for other dyes in the presence of AuNP [27,28]. In contrast, for **AuNPg$_{55}$** no significant changes in the spectra were observed.

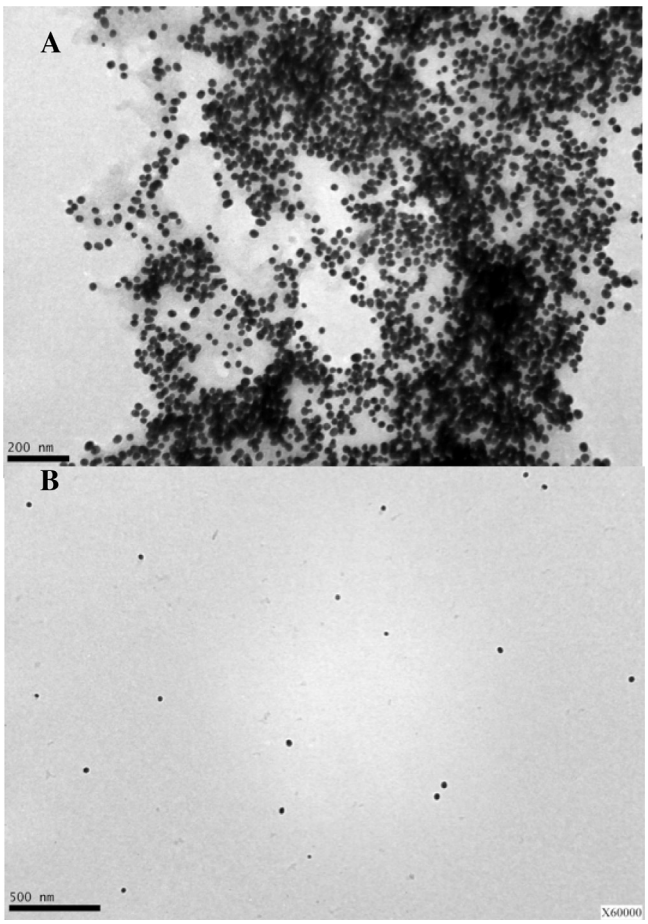

Fig. 2. (A) Representative TEM image for **AuNPc$_{13}$** after addition of 100 μmol L^{-1} **RA** at pH 5.03 showing the presence of agglomerates. (B) TEM image showing the absence of agglomerates for **AuNPc$_{13}$** after addition of 50 μmol L^{-1} **RA** at pH 7.97.

Similarly, **AgNPc$_{52}$** were also more stable at pH 7.97 as no decreases in absorption were observed and zeta potential values (not shown) were larger in the presence of the dye; instead a shoulder at 535 nm appeared in the ΔAbs spectrum (Fig. 1C). This shoulder can also be attributed to an increase in the extinction coefficient of **RA** (as with **AuNPc**) by plasmonic effect in the vicinity of the nanostructure surface [29] as it has been also observed for other organic compounds [28]. Interestingly, in the case of **AgNPg$_5$** (Fig. 1C) and **AgNPg$_{29}$** (not shown) the **RA** absorption was dumped down in the presence of these nanoparticles, indicating the interaction of AgNP with **RA** anion also depends on the ligand at some extend. This can be useful to distinguish the presence of different AgNP in a mixture.

These results suggest in conjunction with those obtained at pH 5.03 the interaction with **RA** depends on NP size and nature of the metal as expected, and also on the ligand identity. Furthermore, these outcomes (Table 1) resulted very promising for the use of **RA** to differentiate in a mixture **AgNPc** from **AuNPc** at pH 5.03 and 7.97; or **AgNPc** from **AgNPg** a pH 7.97, the pairs of NP that showed larger spectroscopic differences.

3.1.3. Interaction with *BF*

Analysis of the corresponding ΔAbs_{net} spectra showed the existence of interaction between **BF** with **AuNPc** and **AgNPc**. For **AuNPc$_{13}$**, a new band at *ca.* 650 nm appeared whereas for **AgNPc$_{52}$** depletion of the absorption at 425 nm was observed together with a new band at *ca.* 705 nm (Fig. 3). In a similar fashion, TEM images (not shown) revealed the presence of **BF** induces the formation of

Table 1
Summary of maximum spectroscopic changes observed for NP in the presence of **RA** and **BF**.

Dye	pH (buffer)	Type of NP	Max sensitivity wavelength[a]/nm	Suitable composition of NP mixtures[b]
RA	5.03 (citrate)	**AgNPc**	425 (−)	**AgNPc:AuNPc**
		AuNPc	570 (+)	
		AgNPg	425 (−)[c]	
		AuNPg	478 (−)[c]	
	7.97 (phosphate)	**AgNPc**	530 (+)	**AgNPc:AuNPc** **AgNPc:AgNPg**
		AuNPc	540 (+)	
		AgNPg	530 (−)	
		AuNPg	No change	
BF	6.00 (water)	**AgNPc**	425 (−)	**AgNPc:AuNPc**
		AuNPc	650 (+)	
		AgNPg	No change	
		AuNPg	No change	

[a] Corresponds to the wavelength where the ΔAbs_{net} is maximum. The sign between parentheses indicates the sign of the change in Absorbance respect to the NP in the absence of dye.
[b] This composition corresponds to the pair of NP where each single NP in the indicated mixture can potentially be detected based on the observed spectroscopic changes in the presence of dye.
[c] No significant.

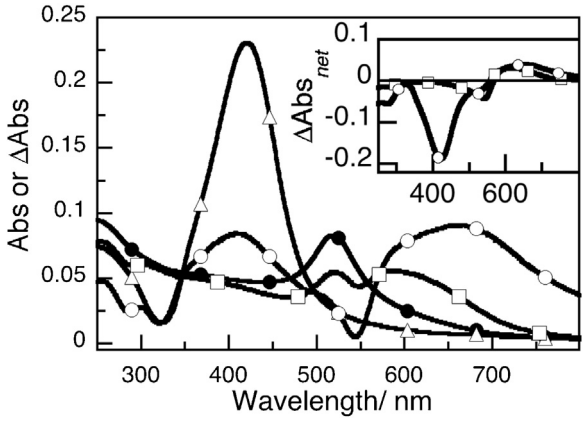

Fig. 3. Absorption spectra for (△) **AgNPc$_{52}$** (0.06 nmol L^{-1}), (●) **AuNPc$_{13}$** (0.37 nmol L^{-1}) and their corresponding ΔAbs spectra for (○) **AgNPc$_{52}$** and (□) **AuNPc$_{13}$** obtained with 5 μmol L^{-1} **BF** in deionised water. Inset shows their corresponding ΔAbs_{net}.

NP agglomerates. In addition, interaction was also proved by Surface Enhancement Raman Spectroscopy (SERS) where **AuNPc$_{13}$** and **AgNPc$_{52}$** enhanced the intensities at 1375 cm^{-1} (assigned to C—N and C—C stretching vibrations) [40] and 1524 cm^{-1} (C—C stretching vibrations) [40] of **BF** (Fig. 4).

No significant spectroscopic changes were found with **AgNPg$_5$** and **AuNPg$_{55}$**. From these results, the pair **AgNPc:AuNPc** was chosen as the NP mixture to be differentiated using **BF**. For both kinds of nanoparticles, ΔAbs at selected wavelengths was chosen as the analytical signal.

3.2. Semiquantitative detection of mixtures of nanoparticles using *RA*

Based on the spectroscopy differences observed when **RA** interacts with different metal nanoparticles (Fig. 1, Table 1), **RA** was chosen as a molecular probe to detect mixtures of the following pairs: **AuNPc$_{13}$:AgNPc$_{52}$** at pH 5.03 (Fig. 5C) and 7.97 (Fig. 3A) and **AgNPc$_{52}$:AgNPg$_5$** at pH 7.97 (Fig. 3B). The ΔAbs spectra (Fig. 5) for mixtures of these pairs of nanoparticles at different concentration ratios showed variations respect to ΔAbs spectra containing only one type of nanoparticle (Fig. 1). They were also different compared to the NP mixtures absorption spectra without **RA** (Fig. 5). As it turned out that in these mixtures no single wavelength could be associated only to the contribution of one type of NP, **RA** can be used in a semiquantitative fashion as a rapid screening test to detect the presence of gold and silver nanoparticles mixtures before using a more sophisticated method for their exact quantification. Then, **RA** resulted sensitive to the presence of mixtures of **AuNPc$_{52}$:AgNPc$_{13}$** at pH 5.03 up to a ratio 167:1; 90:1 for **AuNPc$_{13}$:AgNPc$_{52}$** at pH 7.97 and 67:1 for **AgNPg$_5$:AgNPc$_{52}$** at pH 7.97.

3.3. Analytical parameters to determine nanoparticles in mixtures using *BF*

Using **BF** permitted to select a wavelength for each NP type. Thus, the analytical parameters were determined as follows.

Table 2
Analytical parameters determined for mixtures of **AuNPc** and **AgNPc** using **BF** as molecular probe.

Type of NP	Calibration equation: $\Delta Abs^{\lambda} = m \times [NP] + b$		$s_{y/x}$ (n)[f]	LOD/pmol L^{-1}	LOQ/pmol L^{-1}
	Sensitivity (m)/nmol^{-1} L	b			
AgNPc$_{52}$[a]	1.04 ± 0.09	0.008 ± 0.005	0.006 (6)	19 ± 2	57 ± 5
AgNPc$_{52}$[b]	2.26 ± 0.08	0.031 ± 0.003	0.009 (14)	13.1 ± 0.5	39 ± 1
AgNPc$_{52}$[c]	2.28 ± 0.06	0.0515 ± 0.0008	0.002 (10)	2.89 ± 0.08	8.8 ± 0.2
AuNPc$_{13}$[d]	0.21 ± 0.01	0.040 ± 0.003	0.007 (9)	0.108 ± 0.005	0.33 ± 0.02
AuNPc$_{13}$[e]	0.085 ± 0.005	0.175 ± 0.004	0.005 (7)	0.20 ± 0.01	0.61 ± 0.03

Errors informed for m and b are those calculated using the software. Errors for LOD and LOQ were obtained by error propagation.
[a] Calibration performed in the absence of AuNP (ΔAbs^{425}, R^2 = 0.971).
[b] Calibration performed in the presence of 0.20 nmol L^{-1} and 0.44 nmol L^{-1} of **AuNPc$_{13}$** (ΔAbs^{425}, R^2 = 0.984).
[c] Calibration performed in the presence of 0.024 nmol L^{-1} of **AuNPc$_{28}$** (ΔAbs^{425}, R^2 = 0.994).
[d] Calibration performed in the presence of 0.03 nmol L^{-1} of **AgNPc$_{52}$** (ΔAbs^{706}, R^2 = 0.981).
[e] Calibration performed in the presence of 0.10 nmol L^{-1} of **AgNPc$_{52}$** (ΔAbs^{706}, R^2 = 0.985).
[f] Number of data in the linear regression.

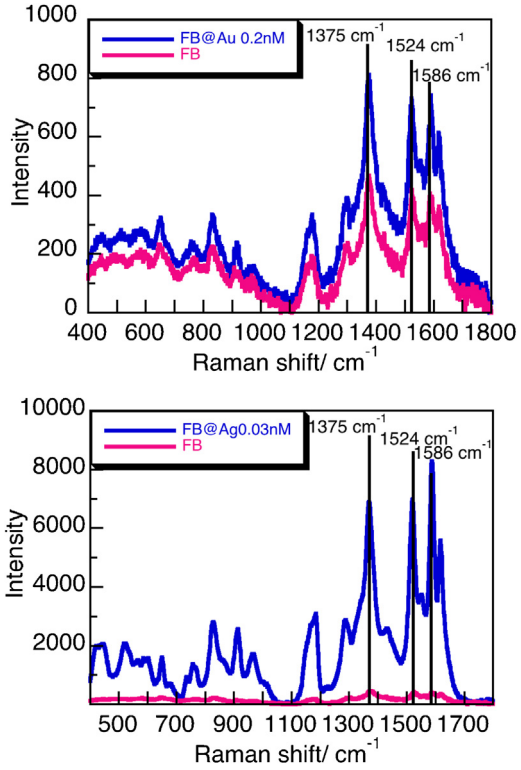

Fig. 4. (Top) SERS spectra for 5 μmol L^{-1} **BF** with and without **AuNPc$_{13}$** (0.2 nmol L^{-1}) (FB@Au and FB, respectively). (Down) SERS spectra for 5 μmol L^{-1} **BF** with and without **AgNPc$_{52}$** (0.03 nmol L^{-1}) (FB@Ag and FB, respectively. Indicated signals correspond to C—C (1375, 1524 and 1586 cm^{-1}) and C—N (1375 cm^{-1}) stretching frequencies.

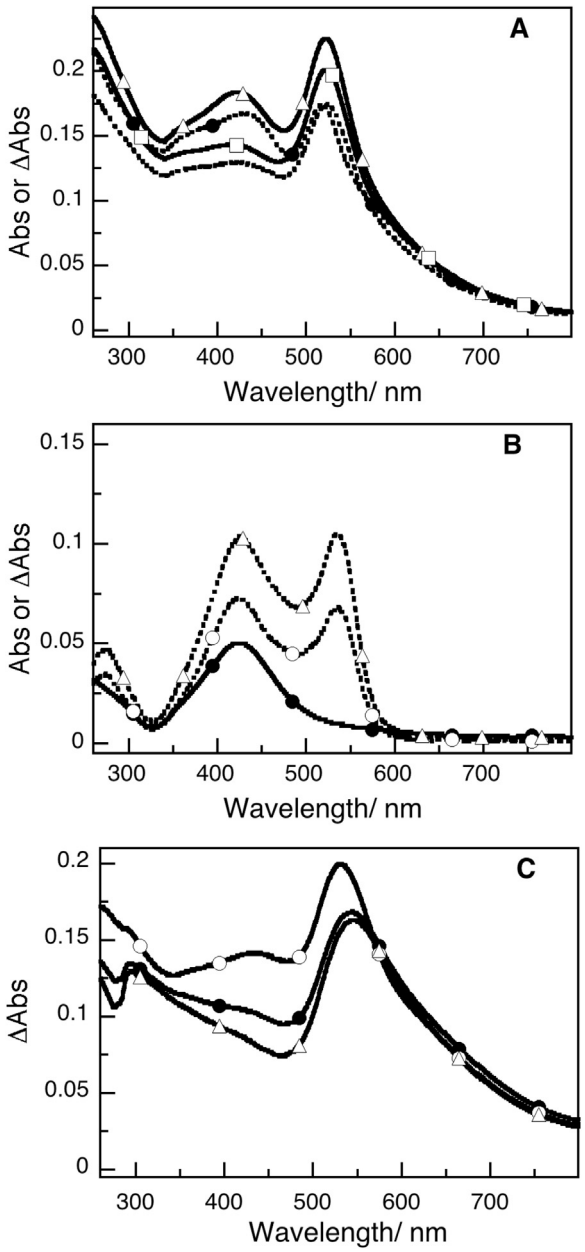

Fig. 5. (A) ΔAbs spectra for mixtures of **AuNPc$_{13}$** (0.81 nmol L^{-1}) and **AgNPc$_{52}$** at pH 7.97 obtained with 50 μmol L^{-1} **RA** at **AgNPc$_{52}$:AuNPc$_{13}$** ratios of (□) 0.011 and (△) 0.023 compared to the corresponding absorption spectra for the mixtures of nanoparticles without **RA** at **AgNPc$_{52}$:AuNPc$_{13}$** ratios of (––) 0.011 and (–●–) 0.023. (B) ΔAbs spectra for mixtures of AgNPg$_5$ (0.47 nmol L^{-1}) and **AgNPc$_{52}$** at pH 7.97 obtained with 50 μmol L^{-1} **RA** at **AgNPc$_{52}$:AgNPg$_5$** ratios of (○) 0.015 and (△) 0.029 compared to the absorption spectra (●) for the mixture of **AgNPc$_{52}$:AgNPg$_5$** at a ratio of 0.029 without **RA**. (C) ΔAbs spectra for mixtures of **AuNPc$_{13}$** (0.81 nmol L^{-1}) and AgNPc$_{52}$ at pH 5.03 obtained with 100 μmol L^{-1} **RA** at **AgNPc$_{52}$:AuNPc$_{13}$** ratios of (△) 0, (●) 0.006 and (○) 0.022.

The analytical signals employed for **AgNPc$_{52}$** and **AuNPc$_{13}$** were ΔAbs^{425} and ΔAbs^{706}, respectively. We obtained two calibration curves for **AgNPc$_{52}$** at two different levels of **AuNPc$_{13}$** (Fig. 6). In a similar way, we constructed the calibration curves for **AuNPc$_{13}$** at two different levels of **AgNPc$_{52}$** (see Supplementary data, Fig. S9). Table 2 shows the main analytical parameters.

Independently of the **AuNPc$_{13}$** concentration level in the mixture, the relationship was linear in the whole **AgNPc$_{52}$** concentration range (Fig. 6). Therefore, the presence of **AuNPc** did not interfere in the determination of **AgNPc$_{52}$**. Remarkably, a variation in the **AuNPc** size (testing **AuNPc$_{28}$**) showed the same sensitivity for **AgNPc$_{52}$** modifying only the intercept value (Fig. 6 and Table 2). Interestingly, the sensitivity for **AgNPc$_{52}$** in the mixture was doubled in comparison to that obtained in the absence of **AuNPc** (Fig. 6 and Table 2).

The limits of detection (LOD) and quantification (LOQ) were determined as 3.29 s_B/m and 10 s_B/m, respectively [41], where s_B is the standard deviation of the blank and m is the slope of the calibration curve. In this work, the residuals standard deviation of the linear regression data ($s_{y/x}$, Table 2) was used as an estimate of s_B.

For **AuNPc$_{13}$**, both sets of calibration solutions showed a linear dependence for ΔAbs^{706} with the **AuNPc** concentration though they differed in sensitivity depending on the **AgNPc$_{52}$** concentration (Table 2 and Fig. S9 in Supplementary data). As a consequence of this effect, the LOD for **AuNPc$_{13}$** showed dependence with the amount of **AgNPc$_{52}$** present in the sample. The LODs determined in this work for **AuNPc$_{13}$** (Table 2) are equal or lower than the LOD (0.20 nmol L^{-1}) obtained by a method based on quenching of carbon dots fluorescence recently reported for 13 nm **AuNPc** [42].

Although the LODs reported here (8.25 μg mL^{-1} for **AgNPc$_{52}$** and 1.37 μg mL^{-1} for **AuNPc$_{13}$**) are larger in comparison with the best LODs reported in literature for environmental purposes, (*e.g.* 6 ng L^{-1} for AgNP by CPE-ICP-MS [21] and 0.7 ng L^{-1} by CPE-ETAAS [24] and 11.2 μg L^{-1} for AuNP by CE [43]), the proposed method has the following advantages: it does not require any separation step, the presence of free Ag^+ or Au^{3+} ions does not interfere in the analytical signal, and it does not require high skilled personnel. The proposed method can be very useful for a fast detection of NP mixtures in a quite simple way.

On the other hand, though accurate quantification of **AuNPc** is more limited due to the need of knowing first the concentration of **AgNPc**, this could be accomplished in two steps: (1) first, determining the concentration of **AgNPc** using the corresponding calibration

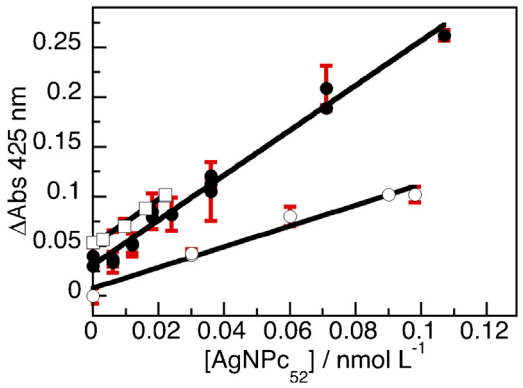

Fig. 6. Calibration curves for **AgNPc$_{52}$** using 5 μmol L^{-1} **BF** as molecular probe in the absence of **AuNPc** (○) and in the presence of **AuNPc$_{13}$** at different concentration levels: 0.20 nmol L^{-1} and 0.44 nmol L^{-1} (●), and **AuNPc$_{28}$** 0.024 nmol L^{-1} (□). Each data was performed by duplicate and error bars indicate the residuals errors.

Table 3
Recoveries of **AgNPc$_{52}$** in drinking water.[a]

Added amount (pmol L^{-1})	Found amount (pmol L^{-1})	Recovery[b] (%)	RSD[b] (%)
11.5	12.5	112	6
16.0	19.0	120	2
22.0	24.7	112	3
26.0	21.5	83	5

[a] 5% (v/v) drinking water, **AuNPc$_{28}$** (0.024 nmol L^{-1}).
[b] Average recovery and relative standard deviation (RSD) calculated from triplicate samples.

parameters and once the **AgNPc** is known, (2) the concentration of **AuNPc** can be estimated using the appropriate calibration parameters.

3.4. Applicability

The method was validated for **AgNPc$_{52}$** by application to recovery assays in drinking water from the Córdoba distribution network (Table 3). The analysis was carried out by MOSA (Method of Standard Additions) to minimize any matrix effect. Recoveries at different levels of fortification satisfy the detection of **AgNPc$_{52}$** in mixtures containing also **AuNPc** in drinking water without any pretreatment. In order to evaluate the accuracy of the method, we calculated the overall average recovery (R) from data in Table 3 as 106.5%, and performed a two-tail test-t. Comparing the experimental t-value with the corresponding $t_{0.05,\,\nu=3}$ which is 3.182, we found that the calculated t-value (0.84) was smaller than the tabulated t-value. Therefore, the null hypothesis (H_0: $R = 100\%$) was accepted with 95% confidence indicating the accuracy of the method.

4. Conclusions

In summary, typical pH indicators **RA** and **BF** were successfully used as sensing systems for the detection of mixtures of metallic nanoparticles semiquantitative and quantitative, respectively. Semiquantitative detection of mixtures containing AgNP with different ligands on the surface was possible using **RA** at pH 7.97 up to a ratio of 67:1 for **AgNPg:AgNPc**. Quantification of **AgNPc** mixed with **AuNPc** can be done using **BF** with satisfactory recoveries (83–120%) in drinking water without previous separation.

The proposed analytical strategy represents a fast, simple and economical method to screen for mixtures of silver and gold nanoparticles in aqueous media and determine their concentration, opening a window for spectroscopic strategies to be exploited. This method also represents an excellent alternative to more sophisticated techniques for the analysis of metal nanoparticles. Furthermore, this methodology is likely to be extended to other nanoparticles mixtures whose ligands are not bound covalently to the metal surface in order to favor a ligand exchange by the molecular probes and to evaluate aqueous environmental samples.

Acknowledgments

This research was supported by grants from the ANPCyT, the SECYT-UNC, the CONICET and the MINCyT-Cordoba. We gratefully acknowledge to undergraduate student Rodrigo Núñez for assistance in some experimental measurements and to Dr. Claudia Nome (CIAP-INTA) and Dr. Luis Fabietti (LAMARX) for technical assistance with some of the microscopy measurements.

Appendix A. Supplementary data

Supplementary data associated with this article can be found, in the online version, at http://dx.doi.org/10.1016/j.snb.2016.01.064.

References

[1] M.E. Stewart, C.R. Anderton, L.B. Thompson, J. Maria, S.K. Gray, J.A. Rogers, R.G. Nuzzo, Nanostructured plasmonic sensors, Chem. Rev. 108 (2008) 494–521.
[2] C. Cobley, J. Chen, E. Cho, L. Wang, Y. Xia, Gold nanostructures: a class of multifunctional materials for biomedical applications, Chem. Soc. Rev. 40 (2011) 44–56.
[3] J.C. Scaiano, K. Stamplecoskie, Can surface plasmon fields provide a new way to photosensitize organic photoreactions? From designer nanoparticles to custom applications, J. Phys. Chem. Lett. 4 (2013) 1177–1187.
[4] S. Kinge, M. Crego-Calama, D. Reinhoudt, Self-assembling nanoparticles at surfaces and interfaces, ChemPhysChem 9 (2008) 20–42.
[5] K. Saha, S.S. Agasti, C. Kim, X. Li, V.M. Rotello, Gold nanoparticles in chemical and biological sensing, Chem. Rev. 112 (2012) 2739–2779.
[6] X. Wang, H. Fan, P. Ren, H. Yu, J. Li, A simple route to disperse silver nanoparticles on the surfaces of silica nanofibers with excellent photocatalytic properties, Mater. Res. Bull. 47 (2012) 1734–1739.
[7] Y. Zhang, H. Fan, M. Li, H. Tian, Ag/$BiPO_4$ heterostructures: synthesis, characterization and their enhanced photocatalytic properties, Dalton Trans. 42 (2013) 13172–13178.
[8] X. Wang, H. Fan, P. Ren, Self-assemble flower-like SnO_2/Ag heterostructures: correlation among composition, structure and photocatalytic activity, Colloids Surf. A Physicochem. Eng. Aspects 419 (2013) 140–146.
[9] G.E. Batley, J.K. Kirby, M.J. McLaughlin, Fate and risks of nanomaterials in aquatic and terrestrial environments, Acc. Chem. Res. 46 (2013) 854–862.
[10] N. Khlebtsov, L. Dykman, Biodistribution and toxicity of engineered gold nanoparticles: a review of in vitro and in vivo studies, Chem. Soc. Rev. 40 (2011) 1647–1671.
[11] M.R. Wiesner, G.V. Lowry, P. Alvarez, D. Dionysiou, P. Biswas, Assessing the risks of manufactured nanomaterials, Environ. Sci. Technol. 40 (2006) 4337–4345.
[12] R. Handy, F. Kammer, J. Lead, M. Hassellöv, R. Owen, M. Crane, The ecotoxicology and chemistry of manufactured nanoparticles, Ecotoxicology 17 (2008) 287–314.
[13] D. Kühnel, C. Nickel, The OECD expert meeting on ecotoxicology and environmental fate—towards the development of improved OECD guidelines for the testing of nanomaterials, Sci. Total Environ. 472 (2014) 347–353.
[14] H. Weinberg, A. Galyean, M. Leopold, Evaluating engineered nanoparticles in natural waters, TrAC Trends Anal. Chem. 30 (2011) 72–83.
[15] A. Howard, On the challenge of quantifying man-made nanoparticles in the aquatic environment, J. Environ. Monit 12 (2010) 135.
[16] H. Zänker, A. Schierz, Engineered nanoparticles and their identification among natural nanoparticles, Ann. Rev. Anal. Chem. 5 (2012) 107–132.
[17] B. Ferreira da Silva, S. Pérez, P. Gardinalli, R. Singhal, A. Mozeto, D. Barceló, Analytical chemistry of metallic nanoparticles in natural environments, TrAC Trends Anal. Chem. 30 (2011) 528–540.
[18] H. Hagendorfer, R. Kaegi, M. Parlinska, B. Sinnet, C. Ludwig, A. Ulrich, Characterization of silver nanoparticle products using asymmetric flow field flow fractionation with a multidetector approach—a comparison to transmission electron microscopy and batch dynamic light scattering, Anal. Chem. 84 (2012) 2678–2685.
[19] T. Mudalige, H. Qu, S. Linder, Asymmetric flow-field flow fractionation hyphenated ICP-MS as an alternative to cloud point extraction for quantification of silver nanoparticles and silver speciation: application for nanoparticles with a protein corona, Anal. Chem. 87 (2015) 7395–7401.
[20] J.B. Chao, J.F. Liu, S.J. Yu, Y.D. Feng, Z.Q. Tan, R. Liu, Y.G. Yin, Speciation analysis of silver nanoparticles and silver ions in antibacterial products and environmental waters via cloud point extraction-based separation, Anal. Chem. 83 (2011) 6875–6882.

[21] J. Liu, J. Chao, R. Liu, Z. Tan, Y. Yin, Y. Wu, G. Jiang, Cloud point extraction as an advantageous preconcentration approach for analysis of trace silver nanoparticles in environmental waters, Anal. Chem. 81 (2009) 6496–6502.
[22] G. Hartmann, T. Baumgartner, M. Schuster, Influence of particle coating and matrix constituents on the cloud point extraction efficiency of silver nanoparticles (Ag-NPs) and application for monitoring the formation of Ag-NPs from Ag^+, Anal. Chem. 86 (2014) 790–796.
[23] A.M. Al-Somali, K.M. Krueger, J.C. Falkner, V.L. Colvin, Recycling size exclusion chromatography for the analysis and separation of nanocrystalline gold, Anal. Chem. 76 (2004) 5903–5910.
[24] G. Hartmann, C. Hutterer, M. Schuster, Ultra-trace determination of silver nanoparticles in water samples using cloud point extraction and ETAAS, J. Anal. At. Spectrom 28 (2013) 567.
[25] R. Thomas, Practical Guide to ICP-MS: A Tutorial for Beginner, Third ed., CRC Press, Boca Raton, 2013.
[26] J. Cookson, The preparation of palladium nanoparticles, Platin. Met. Rev. 56 (2012) 83–98.
[27] W. Ni, H. Chen, J. Su, Z. Sun, J. Wang, H. Wu, Effects of dyes, gold nanocrystals, pH, and metal ions on plasmonic and molecular resonance coupling, J. Am. Chem. Soc. 132 (2010) 4806–4814.
[28] N. Narband, M. Uppal, C. Dunnill, G. Hyett, M. Wilson, I. Parkin, The interaction between gold nanoparticles and cationic and anionic dyes: enhanced UV–visible absorption, Phys. Chem. Chem. Phys. 11 (2009) 10513–10518.
[29] S.K. Ghosh, T. Pal, Photophysical aspects of molecular probes near nanostructured gold surfaces, Phys. Chem. Chem. Phys. 11 (2009) 3811–3844.
[30] N.L. Pacioni, M. González-Béjar, E.I. Alarcón, K.L. McGilvray, J.C. Scaiano, Surface plasmons control the dynamics of excited triplet states in the presence of gold nanoparticles, J. Am. Chem. Soc. 132 (2010) 6298–6299.
[31] P.C. Lee, D. Meisel, Adsorption and surface-enhanced raman of dyes on silver and gold sol, J. Phys. Chem. 86 (1982) 3391–3395.
[32] K. Yoosaf, B.I. Ipe, C.H. Suresh, K.G. Thomas, In situ synthesis of metal nanoparticles and selective naked-eye detection of lead ions from aqueous media, J. Phys. Chem. C 111 (2007) 12839–12847.
[33] W. Haiss, N.T. Thanh, J. Aveyard, D.G. Fernig, Determination of size and concentration of gold nanoparticles from UV–vis spectra, Anal. Chem. 79 (2007) 4215–4221.
[34] A. Amat, A. Arques, M. Miranda, S. Seguí, R. Vercher, Degradation of rosolic acid by advanced oxidation processes: ozonation vs. solar photocatalysis, Desalination 212 (2007) 114–122.
[35] X. Liu, M. Atwater, J. Wang, Q. Huo, Extinction coefficient of gold nanoparticles with different sizes and different capping ligands, Colloids Surf. B 58 (2007) 3–7.
[36] K.G. Stamplecoskie, J. Scaiano, V.S. Tiwari, H. Anis, Optimal size of silver nanoparticles for surface-enhanced Raman spectroscopy, J. Phys. Chem. C 115 (2011) 1403–1409.
[37] A.E. Lanterna, E.A. Coronado, A.M. Granados, When nanoparticle size and molecular geometry matter: analyzing the degree of surface functionalization of gold nanoparticles with sulfur heterocyclic compounds, J. Phys. Chem. C 116 (2012) 6520–6529.
[38] S. Fiuza, C. Gomes, L. Teixeira, M. Girão Da Cruz, M. Cordeiro, N. Milhazes, F. Borges, M. Marques, Phenolic acid derivatives with potential anticancer properties—a structure–activity relationship study. Part 1: methyl, propyl and octyl esters of caffeic and gallic acids, Bioorg. Med. Chem. Lett. 12 (2004) 3581–3589.
[39] G.L. Hornyak, J. Dutta, H.F. Tibbals, A.K. Rao, Introduction to Nanosciences, CRC Press Taylor & Francis Group, Boca Raton, 2008.
[40] W. Li, X. Li, N. Yu, Surface-enhanced resonance hyper-Raman scattering and surface-enhanced resonance Raman scattering of dyes adsorbed on silver electrode and silver colloid: a comparison study, Chem. Phys. Lett. 312 (1999) 28–36.
[41] J. Inczédy, T. Lengyel, A. Ure, A. Gelencsér, A. Hulanicki, Compendium of Analytical Nomenclature (Definitive Rules 1997), Third ed., Blackwell Science, England, 1998.
[42] A. Cayuela, M. Soriano, M. Carrión, M. Valcárcel, Functionalized carbon dots as sensors for gold nanoparticles in spiked samples: formation of nanohybrids, Anal. Chim. Acta 820 (2014) 133–138.
[43] K. Lin, T. Chu, F. Liu, On-line enhancement and separation of nanoparticles using capillary electrophoresis, J. Chromatogr. A 1161 (2007) 314–321.

Biographies

Dr. Natalia L. Pacioni is currently an Assistant Professor and an Adjoint Researcher in the Deparment of Organic Chemistry at the INFIQC–CONICET–Universidad Nacional de Córdoba (Argentina). She obtained her PhD in Chemical Sciences from the Universidad Nacional de Córdoba (2007) and performed a postdoctoral training at the University of Ottawa, Canada (2008–2011). Dr. Pacioni research interests include nanomaterials, supramolecular analytical chemistry, molecular switches and design and development of analytical methods for environmental applications.

Dr. Alicia V. Veglia is currently an Associate Professor and Independent Researcher in the Deparment of Organic Chemistry at the INFIQC–CONICET–Universidad Nacional de Córdoba (Argentina). She obtained her PhD in Organic Chemistry from the Universidad Nacional de Córdoba (1985). Dr. Veglia is the head of the Organic Analytical Chemistry group since 2011. Her research interests include supramolecular analytical chemistry; design, development and applications of sensors and devices for biological, agrochemical and environmental applications.